ELSEVIER

Magnetic Resonance Imaging 22 (2004) 81–91

MAGNETIC RESONANCE IMAGING

Influence of MRI acquisition protocols and image intensity normalization methods on texture classification

G. Collewet[a,*], M. Strzelecki[b], F. Mariette[a]

[a]*Cemagref, Rennes, France*
[b]*Technical University of Lódz, Institute of Electronics, Lódz, Poland*

Received 5 March 2003; accepted 11 September 2003

Abstract

Texture analysis methods quantify the spatial variations in gray level values within an image and thus can provide useful information on the structures observed. However, they are sensitive to acquisition conditions due to the use of different protocols and to intra- and interscanner variations in the case of MRI. The influence was studied of two protocols and four different conditions of normalization of gray levels on the discrimination power of texture analysis methods applied to soft cheeses. Thirty-two samples of soft cheese were chosen at two different ripening periods (16 young and 16 old samples) in order to obtain two different microscopic structures of the protein gel. Proton density and T_2-weighted MR images were acquired using a spin echo sequence on a 0.2 T scanner. Gray levels were normalized according to four methods: original gray levels, same maximum for all images, same mean for all images, and dynamics limited to $\mu \pm 3\sigma$. Regions of interest were automatically defined, and texture descriptors were then computed for the co-occurrence matrix, run length matrix, gradient matrix, autoregressive model, and wavelet transform. The features with the lowest probability of error and average correlation coefficient were selected and used for classification with 1-nearest neighbor (1-NN) classifier. The best results were obtained when using the limitation of dynamics to $\mu \pm 3\sigma$, which enhanced the differences between the two classes. The results demonstrated the influence of the normalization method and of the acquisition protocol on the effectiveness of the classification and also on the parameters selected for classification. These results indicate the need to evaluate sensitivity to MR acquisition protocols and to gray level normalization methods when texture analysis is required.

Keywords: Texture analysis; Classification; Gray level normalization

1. Introduction

Texture analysis methods are used to characterize the spatial distribution of gray level variations within an image [1]. They are useful to quantify the complexity of an image linked to the extent, frequency, and spatial arrangement of these variations. This measurement of complexity can provide information on the structure of the object being imaged. This is true in all kinds of images and especially in MR images. It is worth noting that these techniques can provide information that is not visible to the human eye [2]. Several studies have shown the value of texture analysis in MRI applications. It has been successfully used for the characterization of diseased skeletal muscle [3], for the study of lesions in multiple sclerosis patients [4], for the detection of macroscopic lesions and microscopic abnormalities in the hippocampus [5], and for the monitoring of cell therapy in vivo [6]. Texture analysis has also been used in order to contribute to automatic segmentation in the cerebellum [7], tibia, femur, and knees [8]. In food applications, texture analysis of MR images has been found to be a suitable tool to discriminate food structures according to the storage and processing conditions. For example, the co-occurrence matrix method has been used to classify MR images from cheeses according to their composition and internal structure [9], and from the same database it was also possible to predict the sensory characteristics [10]. Texture analysis methods have also been used to study the structural changes in apples induced by ripening [11] and for the classification of Swiss-type cheeses [12]. However, texture parameters are sensitive to all the acquisition conditions including MR protocols, MR scanners, and MR adjustments

* Corresponding author. Tel.: +33-2-2348-2167; fax: +33-2-2348-2115.
E-mail address: guylaine.collewet@cemagref.fr (G. Collewet).

0730-725X/04/$ – see front matter
doi:10.1016/j.mri.2003.09.001

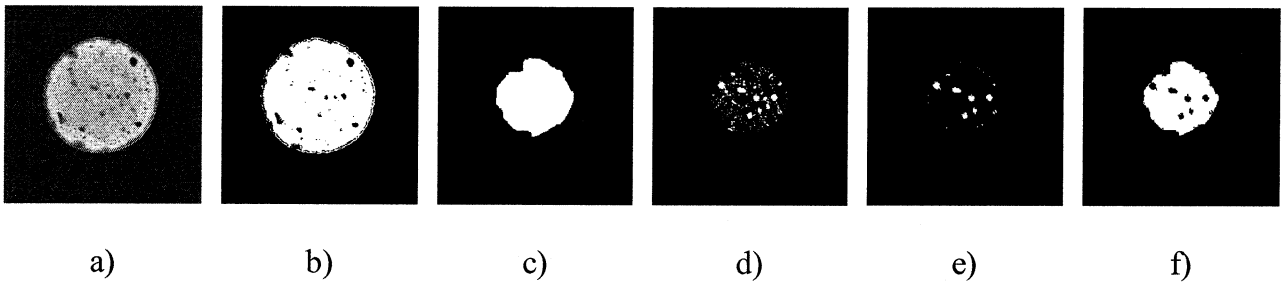

Fig. 1. Creation of the ROI: (a) original image, (b) after thresholding of the background, (c) after closure of the holes and erosion, (d) holes detected by automatic thresholding, (e) holes considered as "artifacts," and (f) final ROI.

[13]. A multi-center trial using reticulated foam gels concluded that the texture measurements were not reproducible between centers [14]. Gray level normalization might be one way of making these methods more reliable.

In this article, we report the influence of two MR acquisition protocols and four gray level normalization methods on the discrimination power of the texture analysis of two classes of food samples. The study analyzed MR images of soft cheeses at different stages of ripening. This choice was based on previous results that showed that the NMR parameters and therefore the MR images were strongly affected by both the microstructural changes of the protein gel and the macroscopic organization inside the cheese induced by the ripening process [15]. Moreover, we have already demonstrated that texture analysis provides full discrimination between ripened and nonripened cheeses [16]. Cheeses should therefore provide good test samples for study.

2. Materials and methods

2.1. Cheeses

The soft cheeses studied were Camembert-type cheeses from the same factory. The cheeses were divided into two groups, the first group comprising nonripened cheeses (about 18 days of ripening), and the second group comprising ripened cheeses (about 43 days of ripening). Sixteen cheeses were analyzed for each group.

2.2. MRI data sets

All the MRI experiments were performed on a 0.2 T MR scanner (Open System; Siemens AG, Erlangen, Germany) with a head coil as receiver coil. During MRI measurements, the cheese samples were maintained at 16 ± 1°C. The MR images were acquired in the plane parallel to the longest cheese surface using a two-dimensional Fourier transform technique. Two different acquisition protocols were used. Both were based on a standard spin-echo sequence with different parameters to produce proton density-weighted images (PDW) (TE = 15 ms, TR = 1500 ms with a bandwidth of 130 Hz/pixel) and T_2-weighted images (T2W) (TE = 80 ms, TR = 1500 ms with a bandwidth of 23 Hz/pixel). One slice located in the middle of the cheese was acquired per cheese, with a field of view of 180 × 180 mm, slice thickness of 4 mm, and matrix size of 256 × 256. The cheeses were analyzed at different periods of time. Twelve (six old and six young) were analyzed by MRI between December 1997 and March 1998, four (two young and two old) in June 2000, and 16 (eight young and eight old) in May and August 2001. The gain and FFT scale parameters were kept constant at each period of acquisition and for each sequence.

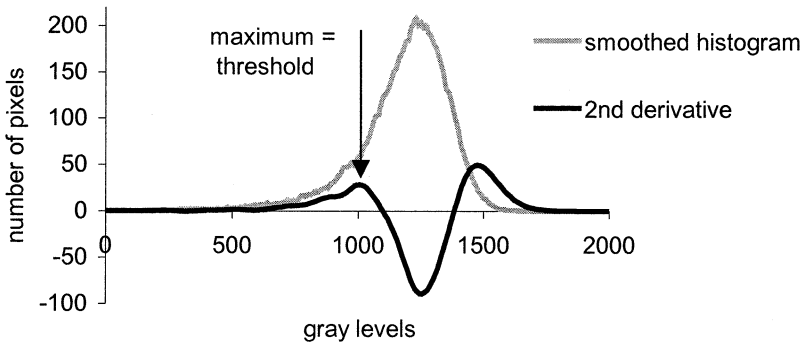

Fig. 2. Automatic computation of the threshold for segmentation of the holes.

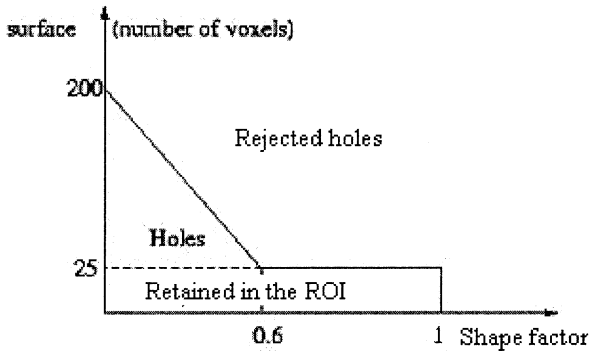

Fig. 3. Boundary between retained and rejected holes.

2.3. Image preprocessing

2.3.1. Construction of regions of interest

Because there are two distinct parts in young cheeses, i.e., the heart, which has not ripened, and the border, which has ripened, regions of interest (ROI) were automatically computed on the PDW images to isolate the areas in the cheeses where the texture measurements were performed. The same ROI was applied to T2W. The ROIs were first reduced to the heart of each cheese. Gas bubbles appeared in the cheeses during ripening, causing black holes in the MR images. A few of them were very large. We checked whether these holes had an effect on the texture parameter values. As they were not statistically representative of the cheese texture we considered them as artifacts and therefore decided to remove them automatically from the ROIs.

The following algorithm was used to compute the ROI on each image:

- Segmentation of the cheese: an automatic thresholding method [17] was used on the original image (Fig. 1a) to separate the background from the cheese. This method considers two classes of gray level values in the image. It computes the threshold value that both maximizes the interclass variance and minimizes the intraclass variance for each image (Fig. 1b). The holes in the thresholded image were then filled using a morphologic operation [18].
- Segmentation of the cheese heart: Twenty iterative erosions with a 3×3 structuring element were applied to ensure that the ROI included only the nonripened part of the young cheese. The same erosions were applied to the old cheese images in order to obtain approximately the same number of pixels for each ROI (Fig. 1c).
- Segmentation of the holes: We considered that the gray levels histogram should be Gaussian in the absence of holes and that the presence of holes induced a change in the left part of the histogram. We analyzed this change and found a threshold value between the hole and cheese pixels. To do this, the gray levels histogram of the original cheese image was computed for the pixels included in the eroded ROI and smoothed using a Shen and Castan filter [19]. The second derivative of the histogram was then computed using two Deriche derivative filters [20] (Fig. 2), and the first local maximum of the second derivative was found, which corresponded to the maximum variation of the histogram slope. This value was used as the threshold for the segmentation of the holes (Fig. 1*d*). The method was validated by visual observation and was considered as acceptable for our purpose.
- Filtration of the holes: Large holes were eliminated according to surface and shape as described in Fig. 3. For each hole, the surface S, the perimeter P, and the shape factor $C = 4\pi S/P^2$ were computed. The holes with high shape factor (>0.6) and a surface above 25 pixels were rejected. In order to discriminate cracks from large bubbles, linear dependency was computed between the hole surface and shape factor (Fig. 3). The holes located in the lower part (Fig. 3) were kept in the ROI. Holes touching the ROI borders were eliminated. An example of rejected holes is presented in Fig. 1*e*.
- The resulting ROI is represented in Fig. 1*f*. Only the pixels in white were taken into account for texture analysis. The number of pixels in the ROIs varied between 5497 and 6568, depending on the images.

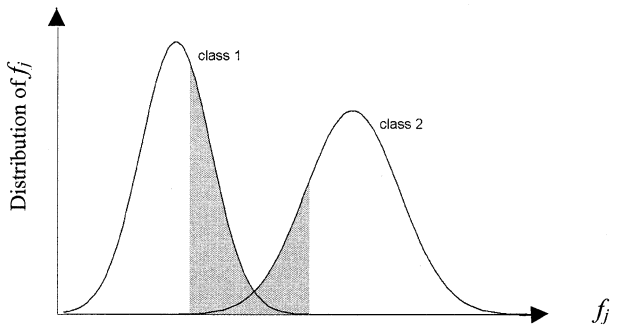

Fig. 4. A sample distribution of feature f_j.

2.3.2. Gray level normalization

Intensities of MR images can vary, even in the same protocol and the same sample and using the same scanner. Indeed, they may depend on the acquisition conditions such as room temperature and hygrometry, calibration adjustment, slice location, B_0 intensity, and the receiver gain value. The consequences of intensity variation are greater when different scanners are used. This relationship must be taken into account for MR image analysis [21,22]. In this study, we considered four schemes for the gray level normalization:

- S1: no normalization was applied. Image intensity was coded with 12 bits in the original images and was quantized to 6 bits to give gray levels between 1 and 64.

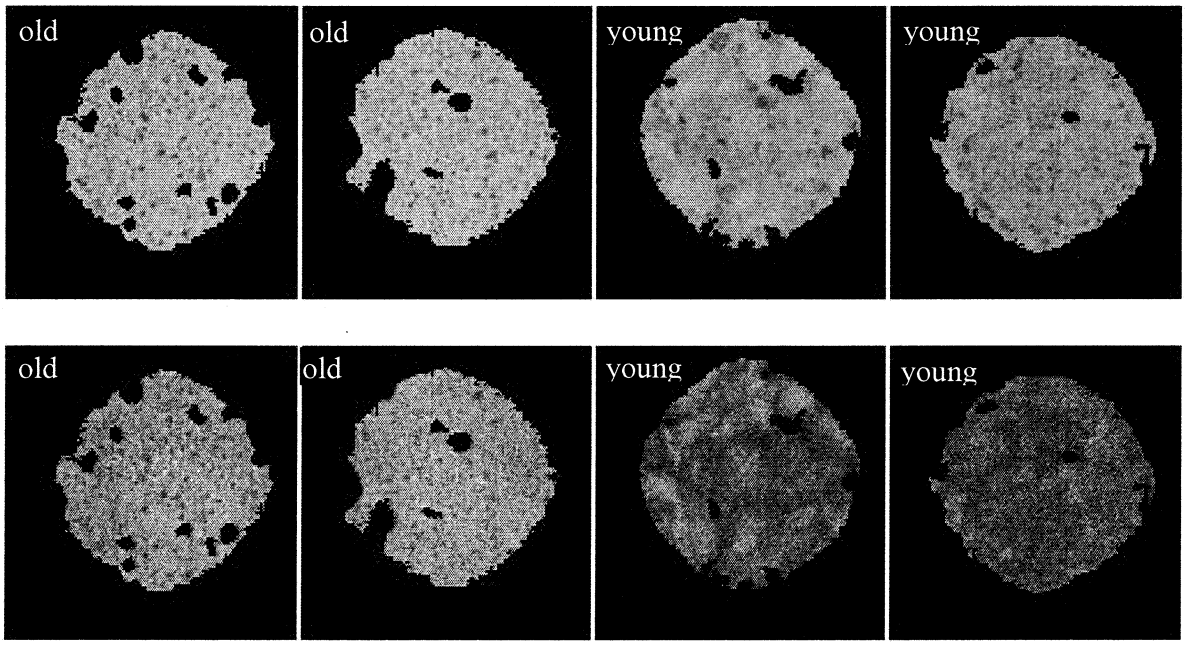

Fig. 5. Top row: ROIs from PDW MR images of two old and two young soft cheeses. Lower row: the same ROIs from T2W MR images. For better visualization, the windowing was different according to the acquisition protocol.

- S2 and S3: we considered here that the variation in image intensity was only multiplicative as observed for example when changing the receiver gain value. Thus we applied a multiplicative transformation to fix the same range of gray levels for all the images of a single protocol using two different schemes. For S2, we applied the same maximum for all the images by multiplying each gray level by the ratio MAXIMUM/(maximum of the current image) where MAXIMUM was a constant. The value of MAXIMUM was arbitrarily chosen at 2000 for both PDW and T2W protocols. This value was higher than the highest maximum value for all the images analyzed. For S3 we applied the same mean for all the images by multiplying each

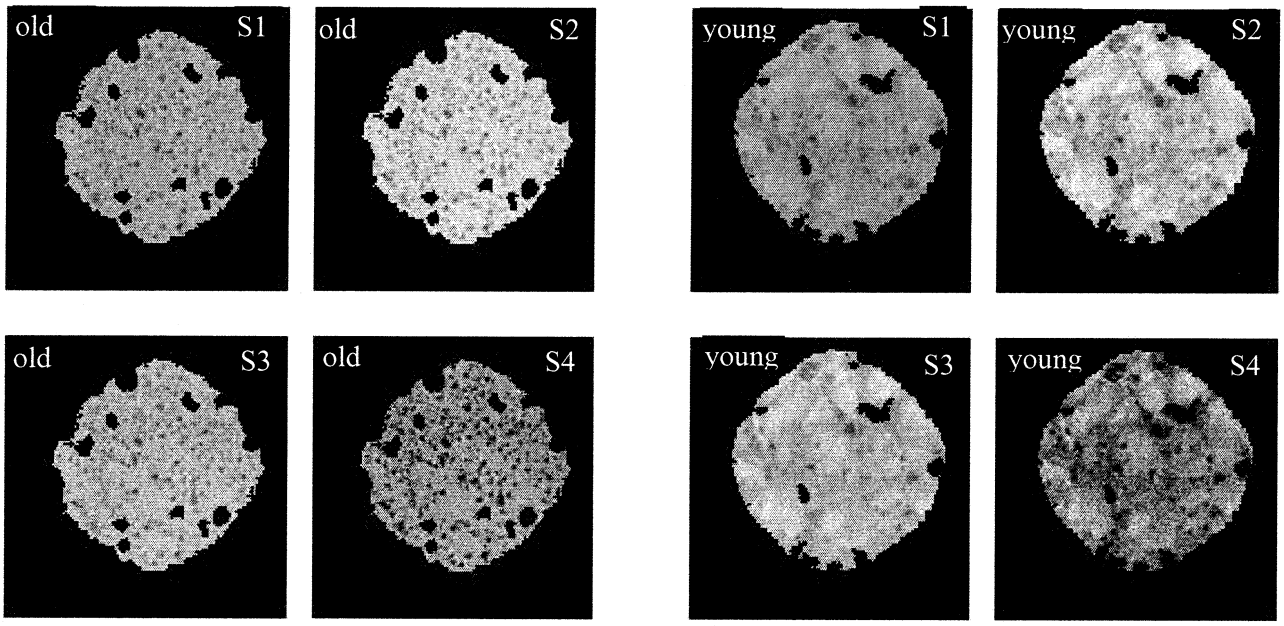

Fig. 6. From left to right and top to bottom: S1, S2, S3, and S4 normalization schemes for one old (cheese on the left) and one young (cheese on the right) on PDW images.

Table 1
POE+ACC coefficients for the four different normalization schemes (S1 to S4) for PDW images

S1		S2		S3		S4	
Feature	*POE + ACC*	*Feature*	*POE + ACC*	*Feature*	*POE + ACC*	*Feature*	*POE + ACC*
S(1,1)Correlat	.000	S(1,1)Correlat	.094	S(1,1)Correlat	.156	135drRLNonUni	.000
WavEnLH_s-2	.301	GrVariance	.153	WavEnLL_s−1	.164	S(1,−1)SumEntrp	.018
S(1,−1)Correlat	.339	S(1,−1)Correlat	.355	WavEnLL_s−4	.245	WavEnHL_s−1	.027
S(1,1)SumEntrp	.472	WavEnHL_s−1	.364	S(1,1)SumAverg	.269	S(1,1)SumEntrp	.159
Teta4	.473	WavEnHH_s−1	.394	S(1,−1)Correlat	.308	Vertl_RLNonUni	.164
Sigma	.485	WavEnLH_s−1	.401	S(1,1)AngScMom	.326	S(0,1)SumEntrp	.178
S(1,0)Correlat	.487	WavEnLH_s−2	.403	S(1,0)SumAverg	.337	WavEnLL_s−4	.184
GrVariance	.499	Sigma	.414	GrVariance	.350	45dgr_RLNonUni	.186
WavEnHL_s−4	.500	135drRLNonUni	.415	WavEnLL_s−3	.356	S(1,1)DifVarnc	.187
S(1,0)Correlat	.516	S(1,0)Correlat	.441	S(1,−1)SumAverg	.373	S(1,0)SumEntrp	.195

gray level by the ratio MEAN/(mean of the current image) where MEAN was a constant. The value of MEAN was the highest mean value for all analyzed images, evaluated separately for PDW and T2W protocols. These two schemes preserve the relative variation between two gray levels because they are purely multiplicative. Finally, intensities were also divided by 64.

- S4: we normalized the image intensities between $\mu \pm 3\sigma$ where μ was the mean value of the gray levels inside the ROI and σ the standard deviation. The gray levels that were located outside the range $[\mu - 3\sigma, \mu + 3\sigma]$ were not considered in further analysis. The range obtained was then quantized to 6 bits, between 1 and 64. This normalization removes the dependency on shift of the mean value and on multiplicative change in the image intensity. Here the relative variation between two gray levels is not preserved.

2.4. Image analysis

Image analysis was performed using Mazda software. This software was developed at the Institute of Electronics, Technical University of Lodz under the COST B11 project "Quantitation of Magnetic Resonance Image Texture" [23] and designed for MR image texture analysis. The following parameters were computed:

- Co-occurrence matrix parameters (i.e., the first 11 parameters defined by Haralick [1]). These parameters were calculated for co-occurrence matrices. These matrices contain probabilities of co-occurrence of pixel pairs with given gray levels, representing the second order image histogram. In this study, such matrices were calculated for interpixel distances equal to one and for four directions: horizontal, vertical, 45°, and 135°. Thus altogether 44 (4 × 11) parameters were evaluated and annotated $S(x,y)$AngScMom, $S(x,y)$Contrast, $S(x,y)$Correlat, $S(x,y)$SumOfSqs, $S(x,y)$InvDfMom, $S(x,y)$SumAverg, $S(x,y)$SumVarnc, $S(x,y)$SumEntrp, $S(x,y)$Entropy, $S(x,y)$DifVarnc, and $S(x,y)$DifEntrp, where $S(x,y)$ corresponded to the co-occurrence matrix for interpixel distance x along the rows and y along the columns. $S(x,y)$ also defined the direction of matrix construction.

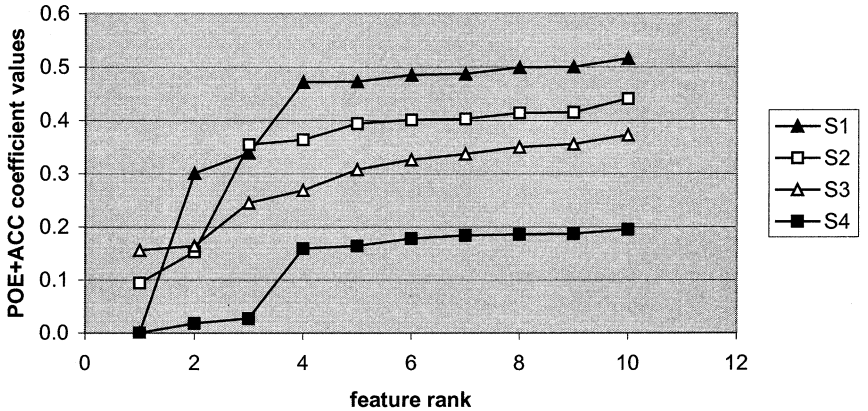

Fig. 7. Evolution of the POE + ACC coefficient for the 10 lowest values for S1, S2, S3, and S4 normalization scheme for PDW.

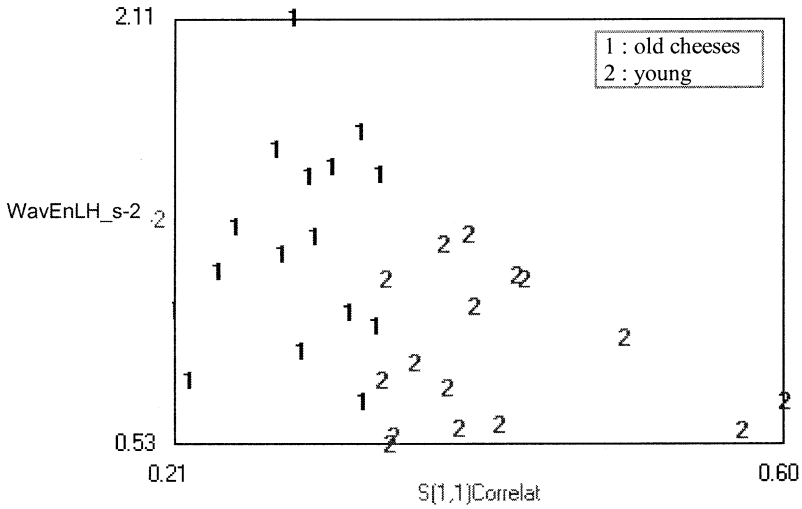

Fig. 8. Data distribution for the two best features by means of POE + ACC method for S1.

- Run-length matrix parameters. The run-length matrix parameters described by Galloway [24] were calculated for four directions, as for the co-occurrence matrix, and provided 20 parameters annotated: *x*_RLNonUni, *x*_GlevNonU, *x*_LngREmph, *x*_ShrtREmp, and *x*_Fraction, where $x \in$ {Horzl, Vertl, 45dgr, 135dgr} depending on the direction considered for computation. The elements of run-length matrix represent the number of times there was a run of length *j* having gray level *i*.
- Gradient matrix (5 parameters). First, the gradient matrix was calculated for the analyzed ROI with a window size of 3 × 3. Based on this matrix, the following parameters were then evaluated: GrMean, GrVariance, GrSkewness, GrKurtosis, and GrNonZeros and represented a distribution of the ROI gradient [25].
- Autoregressive model (first order model) with 5 parameters: Teta1, Teta2, Teta3, Teta4, and Sigma. The autoregressive (AR) model assumes a local interaction between image pixels in that pixel intensity is a weighted sum of neighboring pixel intensities. Assuming image *f* is a zero-mean random field, an AR causal model can be defined as [26]

$$f_s = \sum_{r \in N_s} \theta_r f_r + e_s \quad (1)$$

where f_s is the image intensity at site *s*, e_s denotes an independent and identically distributed (i.i.d.) noise (with standard deviation Sigma), N_s is a neighborhood of *s*, and θ = [Teta1, Teta2, Teta3, Teta4] is a vector of model parameters.
- Wavelet transform (Harr wavelet, 16 parameters). The parameters were annotated WavEnLL_s-1,

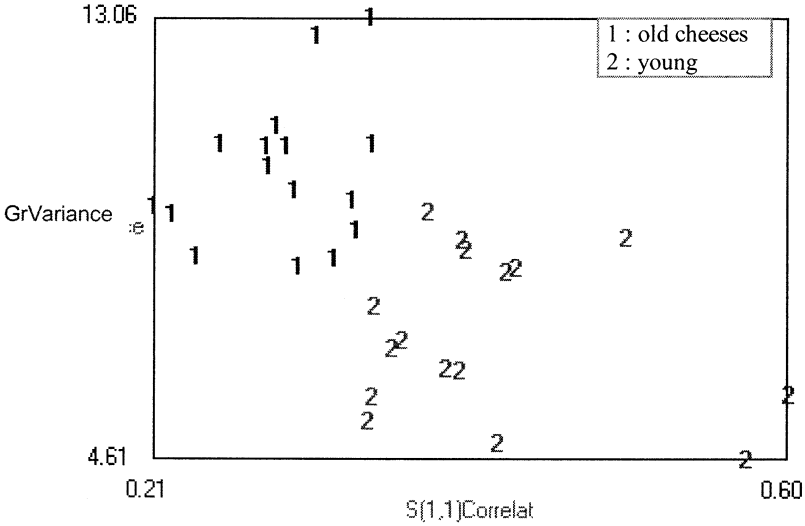

Fig. 9. Data distribution for the two best features by means of POE + ACC method for S2.

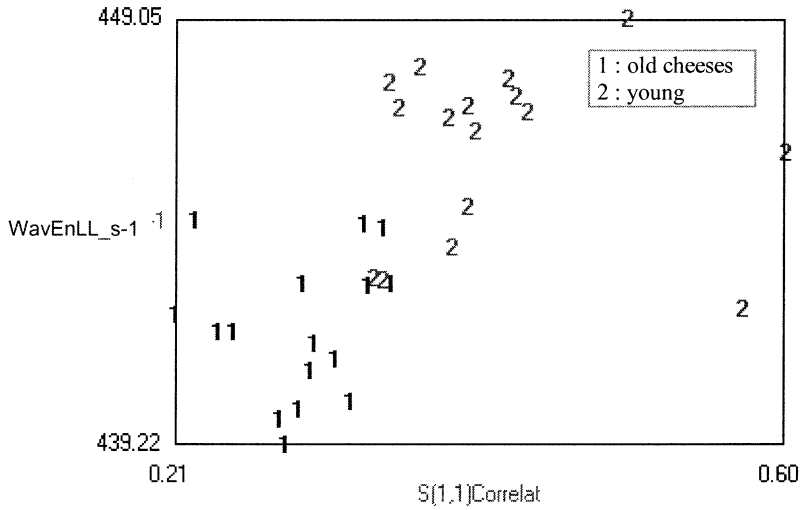

Fig. 10. Data distribution for two best features by means of POE + ACC method for S3.

WavEnLH_s-1, WavEnHL_s-1, WavEnHH_s-1, WavEnLL_s-2, WavEnLH_s-2, WavEnHL_s-2, WavEnHH_s-2, WavEnLL_s-3, WavEnLH_s-3, WavEnHL_s-3, WavEnHH_s-3, WavEnLL_s-4, WavEnLH_s-4, WavEnHL_s-4, and WavEnHH_s-4 and represented an energy of ROI subimages in wavelet coefficients space [27]. The wavelet transform was calculated using Haar basis functions for four image scales, resulting in four subimages for each scale giving altogether 16 parameters.

We decided not to compute the first order parameters such as the mean value of the ROI, because these parameters are not purely texture-descriptive. For example, the same mean value and same standard deviation could be obtained from different textured images [28].

2.5. Feature selection and texture classification

Prior to classification, the number of features was reduced. A large number of features (90) would require a very large number of data samples to provide reliable discriminant analysis results, from the statistical point of view. There was a need for feature reduction to provide the most relevant parameter set for texture discrimination and classification. Feature selection, one of the approaches to feature reduction techniques, is based on the choice of certain features according to a given mathematical criterion. As a consequence, a subset of features that best satisfy such a criterion is obtained. Examples of feature selection methods are the method based on the Fisher criterion and another based on a minimization of classification error and correlation coefficient (POE + ACC). The potential drawback of the Fisher coefficient approach is the possibility of gener-

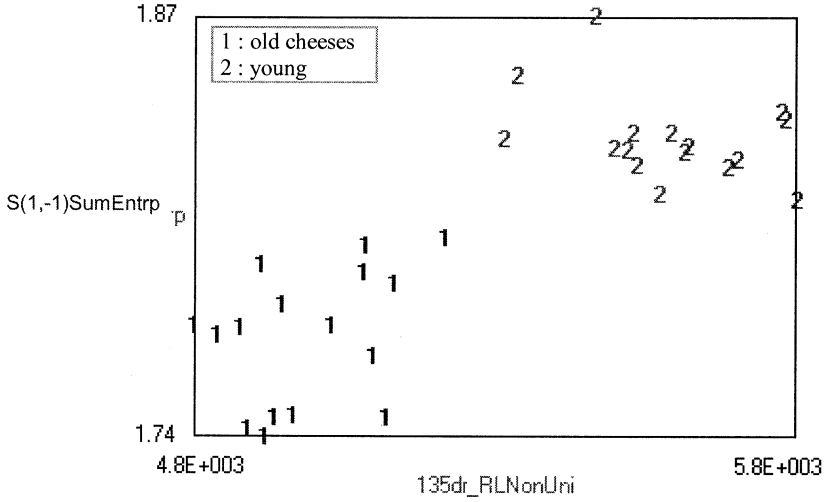

Fig. 11. Data distribution for two best features by means of POE + ACC method for S4.

Table 2
Classification results using 1-NN classifier with the two best features for each normalization scheme in terms of number of misclassified samples for PDW protocol

Normalization scheme	Classification error
S1	4 [12.50%]
S2	1 [3.13%]
S3	4 [12.50%]
S4	0 [0.00%]

ating highly correlated features that possess the same discriminatory properties and, as a consequence, are not useful for classification. The POE+ACC feature selection technique was therefore chosen.

This method is based on minimization of both classification error probability (POE) and average correlation coefficients (ACC) between chosen features [29,30].

The first feature, f_1, is chosen to minimize POE for all classes: $f_1 = f_j{:}\min_j[POE(f_j)]$ where POE(f_j) is the probability of classification error for feature f_j. This probability is defined as a ratio of a number of misclassified samples to the whole number of samples in the analyzed data set, using only feature f_j. Fig. 4 shows sample distribution of feature f_j for two classes. Samples of feature f_j on the left curve belong to class 1, while the samples on the right curve belong to class 2. The samples marked in gray (those for which two curves overlap) can be assigned both to class 1 and 2. In this case, these samples cannot be properly classified. The POE calculated for this feature is given by POE(f_j) = [(*number of misclassified samples*)/(*total number of samples*)]. The next feature is then selected by minimizing the following sum for all features, excluding f_1:

$$f_2 = f_j{:}\min_j[POE(f_j) + |CC(f_1,f_j)|] \tag{2}$$

where $|CC(f_1, f_j)|$ is the absolute value of the correlation coefficient between previously chosen feature f_1 and the new feature f_j. The *n*-th feature is chosen by minimizing the following sum for all remaining features (except for the features already selected):

$$f_k = f_j{:}\min_j\left[POE(f_j) + \frac{1}{n-1}\sum_{k=1}^{n-1}|CC(f_k,f_j)|\right]$$

$$= \min_j[POE(f_j) + ACC(f_j)] \tag{3}$$

where the averaged sum is extended for correlation coefficients between previously selected features and feature f_j. This sum is called an average correlation coefficient (ACC).

The best two features were selected for classification using the nearest-neighbor method described [31]. This classifier is based on a distance calculation between analyzed samples in the feature space. In this paper we assumed an Euclidean distance that is calculated between the given sample and all other samples considered. The analyzed sample is assigned to this class, to which belongs the closest sample in terms of the evaluated distance.

Table 3
Classification results using 1-NN classifier in terms of number of misclassified samples for features selected for S1 normalization scheme for PDW protocol

Normalization scheme	Classification error
S1	4 [12.50%]
S2	6 [18.75%]
S3	5 [15.63%]
S4	14 [43.75%]

3. Results and discussion

3.1. Images

Fig. 5 shows some examples of MR images from old and young cheeses acquired with the PDW and T2W protocols. The black pixels were not taken into account in the analysis as they did not belong to the ROI. Visual examination tended to show that the texture of the young cheeses seemed to be less regular than that of old cheeses. Spots with lower gray levels, which corresponded to small holes or cracks, were regularly distributed in the images of the old cheese while for the young cheeses the appearance was more irregular. However, the difference was not very great. For T2W, the difference was more obvious. There was a contrast between different parts of the young cheeses, while for the old cheeses the paste seemed quite uniform.

3.2. Normalization scheme

Fig. 6 shows PDW ROIs of one old cheese and one young cheese according to the four normalization schemes. The same gray level dynamics were applied to visualize the effects of normalization. S1 and S3 images had almost the same appearance. Normalization scheme S2 tended to increase the brightness, whereas normalization scheme S4 enhanced the contrast. These effects were independent of the stage of ripening and were also observed for the T2W protocol.

3.3. Classification

3.3.1. PDW images

Table 1 summarizes up the POE+ACC coefficients for the four different normalization schemes (S1 to S4). The coefficient values were nil for S1 and S4 normalization and were higher for S2 and S3 normalization schemes when considering the first selected feature. Moreover, the variations in the coefficient values according to the feature rank were dependent on the normalization scheme (Fig. 7). A sharp increase with high coefficient values for the subse-

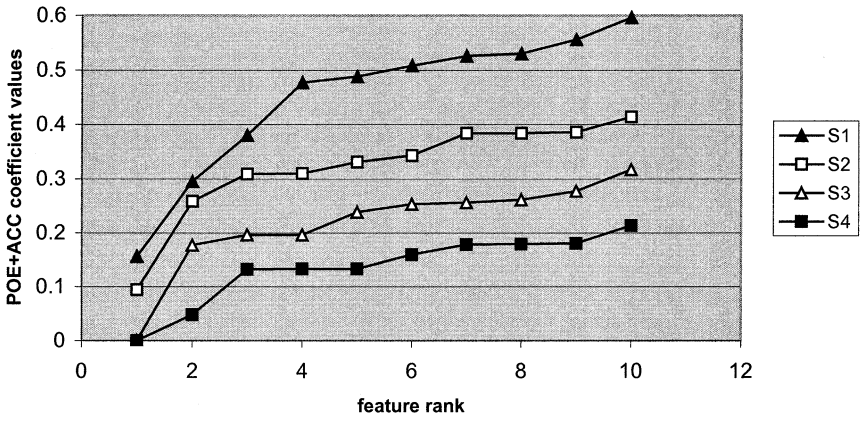

Fig. 12. Evolution of the POE + ACC coefficient for the 10 lowest values for S1, S2, S3, and S4 normalization schemes for T2W.

quent features were observed for S1. For S2 and S3, the same behavior was found with lower coefficient values, and for S4, a small increase was observed for the first three features. Moreover, other features presented stable behavior in relation to the POE coefficient values. This suggests that features selected using S4 normalization were the best for texture classification.

Figs. 8 to 11 show that the separation between the two texture classes was indeed more efficient with the S4 normalization scheme. Classification errors using 1-NN classifier with the two best features for each normalization scheme are presented in Table 2. No classification error was found for S4, while errors remained for S1, S2, and S3.

Depending on the normalization scheme, the best features with regard to the POE + ACC coefficients were not the same. *S*(1,1)Correlat was the best for S1, S2, and S3. Indeed this coefficient is not dependent on multiplicative change in intensity as it represents the correlation between the gray level of one pixel and the gray level of its neighbor. For the S4 normalization scheme, the best coefficient was one from the run-length matrix, which was not considered in the feature selection for S1 to S3. The choice of the coefficient was strongly dependent on the normalization scheme. For example, if the two best features were chosen based on S1 normalization and used for classification when considering S2, S3, or S4 normalization, a considerable increase in classification error was observed (Table 3).

3.3.2. T2W images

Similar behavior was observed for the POE coefficient value according to the normalization scheme (Fig. 12, Table 4). Among all the normalization schemes evaluated, S4 provided the lowest coefficient. However, S3 normalization provided a better coefficient for the first feature compared to that obtained for the PDW protocol. Both S4 and S3 allowed correct classification of the two texture classes (Table 5). For S1 and S2, the *S*(1,−1)Correlat parameter provided the lowest POE coefficient (similar to PDW but using the different co-occurrence matrix direction) (Table 4). These coefficients were highly correlated ($R = 0.99$), and *S*(1,−1)Correlat appeared in fourth and third position for S1 and S2, which shows that the correlation coefficient using interpixel distance (1,1) or (1,−1) was discriminating on both sequences. For S4, the same texture parameter as for PDW was selected as the best for classification. In contrast to the S3 normalization scheme, wavelet parameters were

Table 4
POE+ACC coefficients for the four different normalization schemes (S1 to S4) for T2W images

S1		S2		S3		S4	
Feature	*POE + ACC*	*Feature*	*POE + ACC*	*Feature*	*POE + ACC*	*Feature*	*POE + ACC*
S(1,−1)Correlat	.156	S(1,−1)Correlat	.094	WavEnLH_s−4	.000	135drRLNonUni	.000
Teta4	.295	WavEnHH_s−2	.258	WavEnLL_s−4	.177	WavEnHL_s−1	.048
Teta2	.380	S(1,1)Correlat	.309	WavEnLL_s−1	.196	WavEnHH_s−2	.132
S(1,1)Correlat	.477	WavEnHL_s−4	.310	S(1,−1)Correlat	.196	WavEnLH_s−4	.133
WavEnLH_s−4	.488	Teta4	.331	S(1,1)Correlat	.238	WavEnLL_s−2	.133
S(1,0)Correlat	.508	Teta2	.343	WavEnLL_s−3	.253	Horzl_RLNonUni	.159
GrKurtosis	.526	Sigma	.384	WavEnHL_s−4	.256	S(1,1)DifVarnc	.178
Sigma	.530	WavEnLH_s−4	.384	WavEnLL_s−2	.261	45dgr_RLNonUni	.179
S(1,0)Contrast	.556	S(1,−1)SumAverg	.386	Teta4	.277	WavEnLL_s−4	.180
WavEnHL_s−4	.596	S(0,1)SumAverg	.414	S(1,1)SumVarnc	.317	Veryl RLNonUni	.213

Table 5
Classification results using 1-NN classifier with the two best features for each normalization scheme in terms of number of misclassified samples for T2W protocol

Normalization scheme	Classification error
S1	2 [6.25%]
S2	2 [6.25%]
S3	0 [0.00%]
S4	0 [0.00%]

selected as the best for T2W images and provided perfect classification, whereas this was not the case when considering the PWD protocol.

4. Conclusions

The aim of this study was to evaluate the influence of MRI acquisition protocols and gray level normalization methods on texture classification. Thirty-two MR images from old and young soft cheeses representing two texture classes were acquired using two different MR protocols and analyzed using four normalization schemes. Ninety texture parameters were computed for each image. We then performed feature selection and finally texture classification using a 1-NN classifier. Our results demonstrated the effects of the normalization on both classification performance and on the types of features selected. If no normalization (S1) was performed, the classification errors depended on the MR acquisition protocols. This was also observed when multiplicative normalization (S2, S3) was performed. However, when using "$\pm 3\sigma$" normalization (S4) no relationship was observed, and this normalization provided the best classification results. Enhancement of the variations in gray levels between neighbors in the S4 normalization scheme was a favorable factor for classification performance.

The types of features selected varied according to the normalization scheme. This shows that the choice of the texture parameter should be made according to the normalization scheme being applied. Moreover, this also depended on the acquisition protocol, except for the S4 normalization scheme, for which no relationship was observed.

These results also emphasize the need to use different texture parameters to ensure the lowest number of classification errors. The best parameters for this database were: parameters from the co-occurrence matrix method and wavelet transform for S1, S2, and S3 and parameters from the run-length matrix method for S4.

We therefore suggest checking the sensitivity of the results to the normalization scheme and to the MR acquisition protocol when classification according to texture is required

Acknowledgments

This study was supported financially by the French Ministry of Foreign Affairs and the Polish State Committee for Scientific Research through the Poland-France Scientific Collaboration program Polonium.

References

[1] Haralick RM, Shanmugan K, Dinstein IH. Textural features for image classification. IEEE Trans SMC 1973;3:610–21.
[2] Julesz B. Experiments in a visual perception of texture. Scientific American 1975;34–43.
[3] Herlidou S, Rolland Y, Bansard JY, Le Rumeur E, de Certaines JD. Comparison of automated and visual texture analysis in MRI: Characterization of normal and diseased skeletal muscle. Magn Reson Imaging 1999;17:1393–7.
[4] Yu O, Mauss Y, Zollner G, Namer IJ, Chambron J. Distinct patterns of active and non-active plaques using texture analysis on brain NMR images in multiple sclerosis patients: Preliminary results. Magn Reson Imaging 1999;17:1261–7.
[5] Yu O, Mauss Y, Namer IJ, Chambron J. Existence of contralateral abnormalities revealed by texture analysis in unilateral intractable hippocampal epilepsy. Magn Reson Imaging 2001;19:1305–10.
[6] Eliat P, Lechaux D, Gervais A, et al. Is magnetic resonance imaging texture analysis a useful tool for cell therapy in vivo monitoring? Anticancer Res 2001;21:3857–60.
[7] Saeed N, Puri BK. Cerebellum segmentation employing texture properties and knowledge based image processing: Applied to normal adult controls and patients. Magn Reson Imaging 2002;20:425–9.
[8] Lorigo L, Faugeras O, Grimson W, Keriven R, Kikinis R. Segmentation of bone in clinical knee MRI using texture-based geodesic active contours. in MICCAI. Cambridge, MA: Lecture Notes In Computer Science, 1998.
[9] Mariette F, Collewet G, Marchal P, Franconi JM. Internal structure characterisation of soft cheeses by MRIM. In: Belton P, Hills B, Webb GA, editors. Advances in magnetic resonance in food science. Cambridge, UK: The Royal Society of Chemistry, 1999.
[10] Mariette F, Collewet G, Fortier P, Soulie JM. Relationships between sensory texture of soft cheese and MRI measurements. In: Webb GA, et al, editors. Magnetic resonance in food science. A view to the future. Cambridge, UK: The Royal Society of Chemistry, 2001.
[11] Letal J, Jirak D, Suderlova L, Hajek M. MRI 'texture' analysis of MR images of apples during ripening and storage. Lebensmittel-Wissenschaft und-Technologie 2003;36(7):719–27.
[12] Kim SM, Mc Carthy MJ, Chen P. Determination of structure of eyes and texture of Swiss-type cheeses using magnetic resonance image analysis. J Magn Reson Anal 1996;2:281–9.
[13] Martens H, Thybo AK, Andersen HJ, et al. Sensory analysis for magnetic resonance-image analysis: Using human perception and cognition to segment and assess the interior of potatoes. Food Sci Technol 2002;35:70–9.
[14] Lerski RA, Schad LR, Luypaert R, et al. Multicentre magnetic resonance texture analysis trial using reticulated foam test objects. Magn Reson Imaging 1999;17:1025–31.
[15] Chaland B. Apport de l'IRM bas champ pour l'évaluation des mécanismes d'affinage des fromages pâtes molles et croûtes fleuries. Thesis University of Rennes. 1999.
[16] Collewet G, Strzelecki M, Mariette F. Influence of MRI acquisition protocol on classification of cheese image texture. Magn Reson Materials Biol Phys Med 2002;15:234–5.
[17] Otsu NA. Threshold selection method from gray-level histograms. IEEE Trans SMC 1979;9:62–6.

[18] Serra J. Image analysis and mathematical morphology. London: Academic Press, 1982.
[19] Shen J, Castan S. An optimal linear operator for step edge detection. CVGIP 1992;54:112–33.
[20] Deriche R. Using canny's criteria to derive a recursively implemented optimal edge detector. IJCV 1987;1:167–87.
[21] Nuyl LG, Udupa K. On standardizing the MR image intensity scale. Magn Reson Med 1999;42:1072–81.
[22] Clarke LP, Velthuizen RP, Camacho MA, et al. MRI segmentation: Methods and applications. Magn Reson Imaging 1995;13:343–68.
[23] http://www.EletelP.Lodz.Pl/cost/cost_project.html.
[24] Galloway M. Texture analysis using gray level run lengths. CGIP 1975;4:172–9.
[25] Haralick R. Statistical and structural approaches to texture. Proc IEEE 1979;67:786–804.
[26] Kashyap R, Chellappa R. Estimation and choice of neighbors in spatial-interaction models of images. IEEE Trans Info Theory 1983; 29:60–72.
[27] Porter R, Canagarajah N. A robust automatic clustering scheme for image segmentation using wavelets. IEEE Trans Image Process 1996; 5:662–5.
[28] Materka A, Strzelecki M, Lerski R, Schad L. Toward automatic feature selection of texture test objects for magnetic resonance imaging. 11th Portuguese Conf. on Pattern Recognition RECPAD2000. Porto, Portugal, 2000.
[29] Mucciardi AN, Gose EE. A comparison of seven techniques for choosing subsets of pattern recognition properties. IEEE Trans Computers 1971;20:1023–31.
[30] Dash M, Liu H. Feature selection for classification. Intelligent data analysis 1997;1:131–56.
[31] Shurmann J. Pattern classification: A unified view of statistical and neural approaches. New York: John Wiley, 1996.